Investigate a hybrid open-Rankine cycle small-scale axial nitrogen expander by a camber line control point parameterization optimization technique

Khalil, Khalil; Mahmoud, Saad; Al-Dadah, Raya; Bahr Ennil, Ali

DOI:
10.1016/j.applthermaleng.2017.08.083

Accepted Manuscript

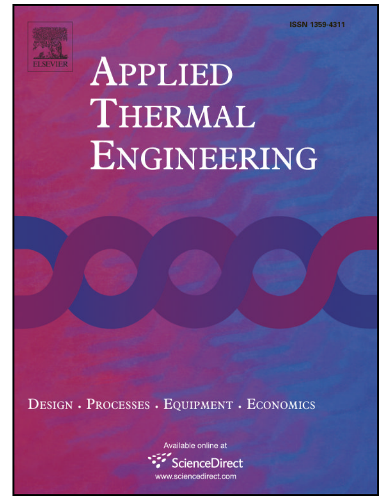

Investigate a hybrid open-Rankine cycle small-scale axial nitrogen expander by a camber line control point parameterization optimization technique

Khalil M. Khalil, S. Mahmoud, R.K. Al- Dadah, Ali Bahr Ennil

PII: S1359-4311(17)30680-4
DOI: http://dx.doi.org/10.1016/j.applthermaleng.2017.08.083
Reference: ATE 10966

To appear in: *Applied Thermal Engineering*

Received Date: 30 January 2017
Revised Date: 27 July 2017
Accepted Date: 18 August 2017

Please cite this article as: K.M. Khalil, S. Mahmoud, R.K. Al- Dadah, A. Bahr Ennil, Investigate a hybrid open-Rankine cycle small-scale axial nitrogen expander by a camber line control point parameterization optimization technique, *Applied Thermal Engineering* (2017), doi: http://dx.doi.org/10.1016/j.applthermaleng.2017.08.083

Investigate a hybrid open-Rankine cycle small-scale axial nitrogen expander by a camber line control point parameterization optimization technique.

Khalil M. Khalil [a,b]*, S. Mahmoud[a], R. K. Al- Dadah[a], Ali Bahr Ennil[a]

[a] The University of Birmingham, Department of Mechanical Engineering, School of Engineering, Birmingham, UK

[b] The University of Baghdad, Mech. Eng. Dept., Iraq

Abstract

During the last few decades, low-grade heat sources such as solar energy and wind energy have enhanced the efficiency of advanced renewable technologies such as the combined Rankine cycle, with a significant reduction in CO_2 emissions. To address the problem of the intermittent nature of such renewable sources, energy storage technologies have been used to balance the power demand and smooth out energy production. In this study, a detailed thermodynamic analysis of a hybrid open Rankine cycle was conducted by using engineering equation solver (EES) software in order to investigate the performance of such a cycle using a liquid nitrogen energy storage system. In this cycle configuration, the conventional closed loop Rankine cycle (topping cycle) is combined with a direct open Rankine cycle (bottoming cycle) for a more efficient system which can solve the problem of discontinuous renewable sources. In the direct open-Rankine cycle, the small expander is the main component that can improve the cycle's performance and as a result, this small expander needs to be optimized for maximum efficiency to achieve high system performance levels. In this work a small-scale nitrogen axial expander has been optimized and modeled to be incorporated into a hybrid open-Rankine cycle, using a one-dimensional preliminary design and CFD three-dimensional ANSYS design exploration and a novel camber line control point parametrization technique, which is outlined in detail. The design optimization approach has been proven as an effective tool that could enhance turbine efficiency from 72% to 76.3% and output power from 2076W to 2597.6 W. The optimized turbine using the control points' approach could also improve the cycle's thermal efficiency by 3.38% compared with the baseline design. Such results underline the potential of full simulation optimization by using a blade camber line control point's parametrization technique for a small-scale expander with low flow rate and rotational speed.

Highlights:-

1. 1D and 3D CFD analysis for nitrogen axial turbine was carried out.
2. Novel camber line control point parametrization technique outlined in details.
3. Enhancing the performance of both the turbine and the hybrid open-Rankine cycle.
4. Small scale axial turbine with high efficiency.
5. Excellent agreement between the current CFD results and experimental work from literatures.

6. Introduction

It is essential, for the sake of developing a sustainable economy to create new energy sources; as in the near future, most fossil power production will be replaced by renewable energy sources, such as the wind or solar power which are available only intermittently in nature [1]. One of the most pertinent impacts of this trend is the increased importance of energy storage systems, which can be utilized to balance peaks of energy from renewable sources. In addition to energy storage power generation systems which smooth out energy production and also reduce energy prices, they enable the increased use of green power production, black-start services, spinning reserves, and cooling applications. The energy storage can be achieved using different technologies such as pumped storage hydropower (PSH), compressed air energy storage (CAES) and cryogenic energy storage (CES). The PSH uses mature storage technology which now makes 95 GW of the worldwide demand; on the other hand the CAES technology is growing and for example, the McIntosh site in Alabama generates 226 MW of electricity using this technology [2, 3]. Cryogenic energy storage (CES) is an innovative proposal for energy storage technology which shows great potential because it depends on the developed and established technologies such as gas liquefaction plants which produce the liquid phase (cryogen). This offers geographically unrestricted plants, a reduction in volume; and freedom in the transportation of the storage medium, compared to PSH and CAES technologies [4]. Some researchers are working on an open expansion cycle [5] and others work with the Rankine cycle [6, 7], in both cases, the thermal efficiency is still low. Based on thermodynamic principles, a Carnot cycle at a temperature lower than 673.15K has a low efficiency of recovering waste heat [8]. Consequently, combining a low-level heat source (closed loop Rankine cycle) with a direct expansion cycle, which uses liquid nitrogen, would appear to be an attractive scheme for converting thermal energy into electrical energy. Several studies were carried out to investigate the combined cycles by focusing on the selection of appropriate combinations Table 1 demonstrates a literature using combined cryogen cycle with a range of working fluids.

Table 1.
literature for combined cryogen cycle

Author	Working fluid	Cycle arrangement	Results
Feifei and Zhang [9]	Liquid Natural Gas LNG, nitrogen, water ammonia	combining an open expansion, Brayton cycle, Rankine cycle	the thermal efficiency of scheme 1 is 60.94%, for scheme 2 is 60%
Li et al. [10]	Methane, ethane, propane, water, ethane, LNG	cascading Rankine cycle, hybrid open-Rankine cycle	Combination of open expansion and the Rankine cycle is more attractive for low heat source
Guizzi et al. [11]	Air, propane, methane,essotherm 650	stand-alone air liquefaction and power recovery plant	Round-trip efficiency of around (50-60%)
Li et al. [12]	water, nitrogen, methane, Thermal-oil 66	integrated solar-cryogen hybrid power system	Integrated system can increase the power by 30% compared to the two solar and cryogen systems acting separately
Chen et al. [13]	Air	air liquefaction and power recovery plant for a propeller	Round-trip efficiency reaches 50%
Khalil KM et al.	Air, Nitrogen	Air liquefaction and two	the thermal efficiency of scheme 1 is

[14]		schemes power recovery plant for nitrogen and air	63.27%, for scheme 2 is 84.15%
Kishimoto et al. [15]	Air, flue gas	combine a gas turbine cycle with a liquid air storage system	Round-trip efficiency reaches 77%
Li et al. [16]	Air, flue gas, nitrogen, oxygen, helium	combine a gas turbine cycle with a liquid nitrogen storage system and CO_2 captured as dry ice	Round-trip efficiency reaches 70%
Kantharaj et al. [17]	Air	Integrated liquid air energy store (LAES) with (CAES)	Round-trip efficiency reaches 67%
Li et al. [18]	Steam, air	integration of nuclear power generation and a CES subsystem	Round-trip efficiency reaches 71.2%
Abdo et al. [19]	Air	air liquefaction two types and power recovery plant	The CES-Claude liquefaction system has higher efficiency than the CES-Linde-Hampson system and cheaper than CES-Collins system
Li et al. [20]	nitrogen, LNG, air, flue gas	combining an open expansion, Brayton cycle	Round-trip efficiency reaches 64%
Morgan et al. [21]	Air	stand-alone air liquefaction and power recovery plant	Round-trip efficiency reaches 60%
Smith [22]	Air, water, Freon	Cryo-storage power plant	Round-trip efficiency reaches 72%

As can be seen from the previous review, all published work is related to cryogenic combined cycle's large-scale systems with a power rating of 2 to 20 MW and a high turbine pressure ratios (300 to 100) therefore achieving high-efficiency levels [9–22]. However, this work investigates small distributed systems for domestic and small building applications with a power rating of 1 to 10 kW, the inlet turbine pressure is ranged from 1.5-3 bar [23]. This small pressure ratio with a small expansion device leads to a low-efficiency expander and low cycle performance levels [24].

There are two expander types: the first one is a positive displacement or volumetric type, such as screw expanders, scroll expanders, or rotary expanders. The other type is a velocity one, such as radial in flow turbines and axial flow turbines [25, 26]. The main advantages for the scroll expander are the small number of moving parts, low noise, low vibration, low flow rate, higher pressure ratio, and working in two-phase conditions [27-29]. The main disadvantages are leakage and friction, the leakage problem needs reliable and effective seals while the friction one needs lubricant compatible with working fluid [30]. Regarding the velocity type expanders, they operate at high rotational speed, thus there is a need for special bearings, but they have the advantages of good manufacturability for compact structure, high efficiency, and high enthalpy drop within single stage [31]. In this work, the axial flow turbine has been chosen because it tolerates operating at low-pressure ratios, as required for the domestic application.

To improve the small cryogenic cycle performance, the design of the small expander needs to be improved and optimized for higher efficiency levels. In this regard, there has been limited work published on the modeling and optimization of small-scale cryogenic turbines, which are key components of the output power cycle. The efficiency of small expanders is relatively low compared to large steam and gas turbines and there is further work needed in this area to achieve an efficient turbine with a power rating of 1-10kW [31]. The designs of small expanders are conducted with a similar approach to large gas and steam turbines, based on one-dimensional mean line and through-flow analysis. However, these design approaches were made based on simplified assumptions and empirical correlations of real tests of large gas turbines for aero engines' application, leading to unsuccessful performance predictions in small turbines [32].

Recently, CFD modeling coupled with a multi-objective genetic algorithm (MOGA) has been proven as an effective optimization tool in turbine design [33 - 36]. Qin et al [33] have carried out genetic algorithm (GA) optimization for a flow path with a mean radius for the axial flow steam turbine stage; the numerical results of which show that this approach is effective for solving problems of the flow path of an axial flow steam turbine stage group where the stage efficiency can be enhanced from 0.85 to 0.87. Ali et al. [34] used a systematic approach for loss prediction in a small-scale axial air turbine, using CFD simulation coupled with a multi-objective genetic algorithm (MOAG) for the turbine rotor, with improvements in turbine efficiency by 12.48%. Rahbar et al. [35] have compared numerical optimizations for single stage supersonic and two stage transonic radial turbines and the results show that turbine isentropic efficiency was enhanced by 15.7% and the power of 10.63 kW. Al Jubori et al. [36] have studied optimization for an organic small-scale axial turbine in the Rankine cycle by using CFD multi-objective genetic algorithm (MOAG) with six organic fluids. The results show that the optimum thermal cycle efficiency is 10.5% and an enhancement in the turbine of 14.08% for working fluid R123.

In this paper, a small-scale nitrogen axial expander has been optimized and modeled to be incorporated into a hybrid open-Rankine cycle using a one-dimensional preliminary design and CFD three-dimensional ANSYS design exploration. The three-dimensional CFD optimization of the small-scale axial expander design at low flow rate (0.1 kg/s) and low rotational speed (20000RPM) is considered to be a difficult task. The technique of optimization using control points along the camber line was used to investigate the best blade shape and dimensions, by taking the maximum total efficiency and output power for the turbine as objective functions. In addition to take blade profile parametrization through changes the control points along the camber line of the thickness and angle of the blades at these points, the number of blades in the stator and rotor, the trailing and leading edges of both rotor and stator blades and the tip clearance thickness in the rotor also have been taken into account. Moreover, a numerical simulation model of the hybrid open expansion- Rankine cycle was designed and modeled in order to predict the effect of the expander's efficiency on the cycle performance. The preliminary design was developed by using engineering equation solver (EES) software [37] to produce the passage's initial dimensions.

7. Thermodynamic modeling of the hybrid open-Rankine cycle system

Based on open expansion and Rankine cycles the proposed scheme Figs.1 uses the cold energy of liquid nitrogen and low-level waste heat. The scheme Fig.1 combines two cycles of nitrogen open expansion and a propane Rankine cycle. The main components of the system are the heat exchanger, evaporator, pumps, and expanders.

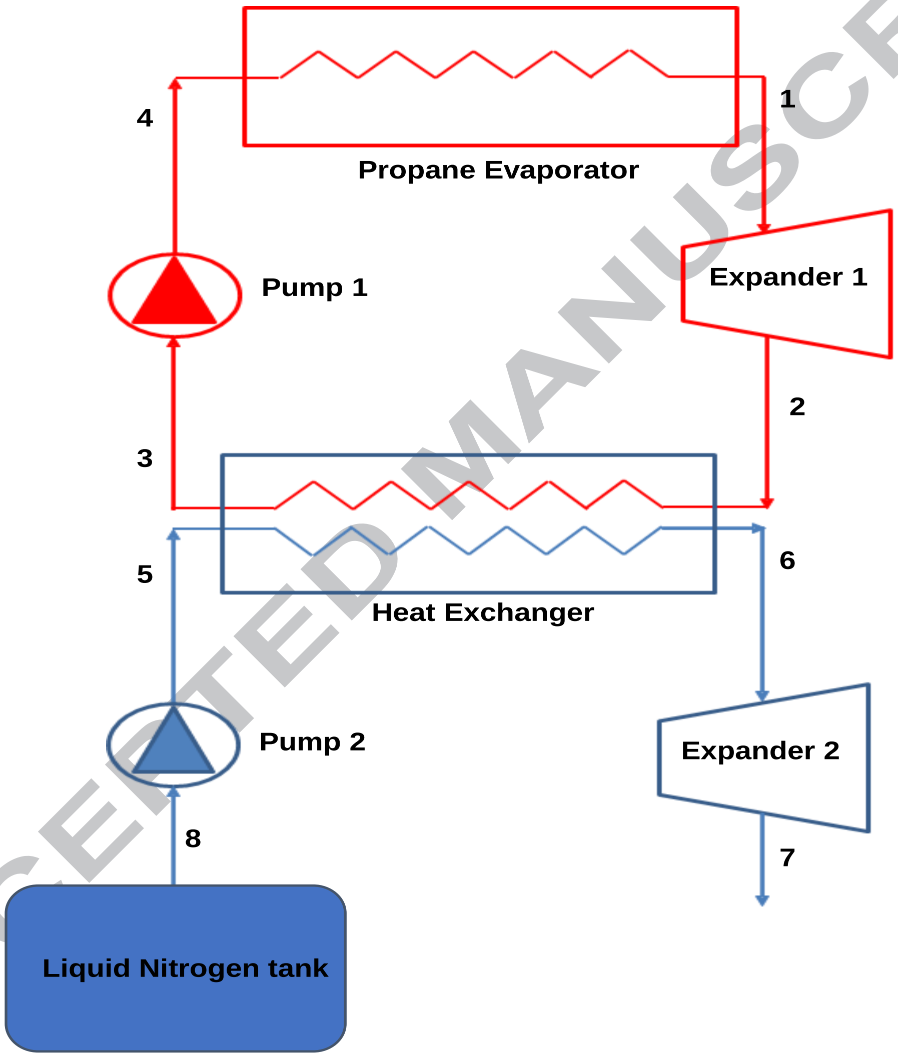

Fig.1. Schematic diagram of hybrid open-closed Rankine cycle

The first stage of the operation is a propane Rankine cycle; see Fig.2 A, which is driven by a low waste heat source and cold energy from the open expansion cycle. The liquid propane is pumped to high pressure by pump#1(3-4) and then flows into an evaporator for heating and vaporization (4-1). After heating, the propane gases generate output work through expanding in expander#1 (1-2). The low-pressure propane flows into a heat exchanger to be condensed by counter current low-temperature liquid nitrogen (2-3). The nitrogen open expansion cycle in Fig.2 B is driven by waste heat from the propane Rankine cycle (topping cycle) and liquid nitrogen cold energy. The liquid nitrogen is generated by gas liquefaction process where the off-peak electricity and/or wind turbine electricity are used to compress the atmospheric air. Then the compressed air is cooled through the cryogenic heat exchanger and then passed through a cryo-turbine, the expansion in the cryo-turbine produces liquid nitrogen and liquid oxygen. Liquid Nitrogen will be charged to tanks of various capacities in terms of volume and pressure and then delivered to various applications. The low-temperature liquid nitrogen is compressed (8-5) to the required pressure by pump#2and then flows to a heat exchanger (5-6). After heating by waste heat from the Rankine cycle, the nitrogen gas, now at the required temperature and pressure, produces work through the expander#2 (6-7). The subcritical cycles are considered in this study to avoid the need for high pressure and so alleviate the safety issues and complexity of the system. The saturated liquid is assumed to be from the Rankine heat exchanger and the pressures with heat losses through the connecting pipes are neglected. Also, the system is assumed to work under steady state conditions. Table2 lists the hybrid open-Rankine cycle input variables with their units and values. Equations (1-4) show the governing equations for pumps through processes (3-4, 8-5) assuming an isentropic efficiency η_{pump}[38]:

$$h_4 = h_3 + \frac{h_{4\_s} - h_3}{\eta_{pump1}} \tag{1}$$

$$h_5 = h_8 + \frac{h_{5\_s} - h_8}{\eta_{pump2}} \tag{2}$$

$$W_{pump1} = h_4 - h_3 \tag{3}$$

$$W_{pump2} = h_5 - h_8 \tag{4}$$

From these equations, it is clear that increasing the pump efficiency will decrease the work required to derive the pump which enhances cycle performance.

Equations (5-8) show the governing equations for the expanders through processes (1-2, 6-7) assuming an isentropic efficiency $\eta_{expander}$:

$$h_2 = h_1 - (h_1 - h_{2s})\eta_{expander1} \tag{5}$$

$$h_7 = h_6 - (h_6 - h_{7s})\eta_{expander2} \tag{6}$$

$$W_{expander1} = h_1 - h_2 \tag{7}$$

$$W_{expander2} = h_6 - h_7 \tag{8}$$

In addition, from the Eqs (5-8) the thermodynamic property enthalpy (h) can be specified by the temperature and pressure for the isentropic state (h_s) and for the actual one (h). Increasing expander efficiency will increase the work extract from expanders which will enhance the cycle performance. The work required to derive these pumps is lower than work extracts from expanders due to phase change process.

Equation (9) shows the heat exchanger effectiveness:

$$E = \frac{Q}{Q_{max}} \tag{9}$$

The heat added to the evaporator is modeled by:

$$q_{in} = h_1 - h_4 \tag{10}$$

The net output work from the combined cycle is:

$$W_{net} = \left(W_{expander1} + W_{expander2}\right) - \left(W_{pump1} + W_{pump2}\right) \tag{11}$$

The combined cycle's thermal efficiency is then determined by:

$$\eta_{thermal} = \frac{W_{net}}{q_{in}} \tag{12}$$

It can be seen from Eq (6) that increase cryogenic expander isentropic efficiency ($\eta_{expander2}$) will decrease the enthalpy at this expander output (h_7), that will increase power output from expander2 according to equation (8). Increasing cryogenic expander work output will increase the (W_{net}) specific total network extract from the combined cycle as shown above in Eq (11) which in turn increase the thermal efficiency ($\eta_{thermal}$) for the combined cycle according to Eq(12).

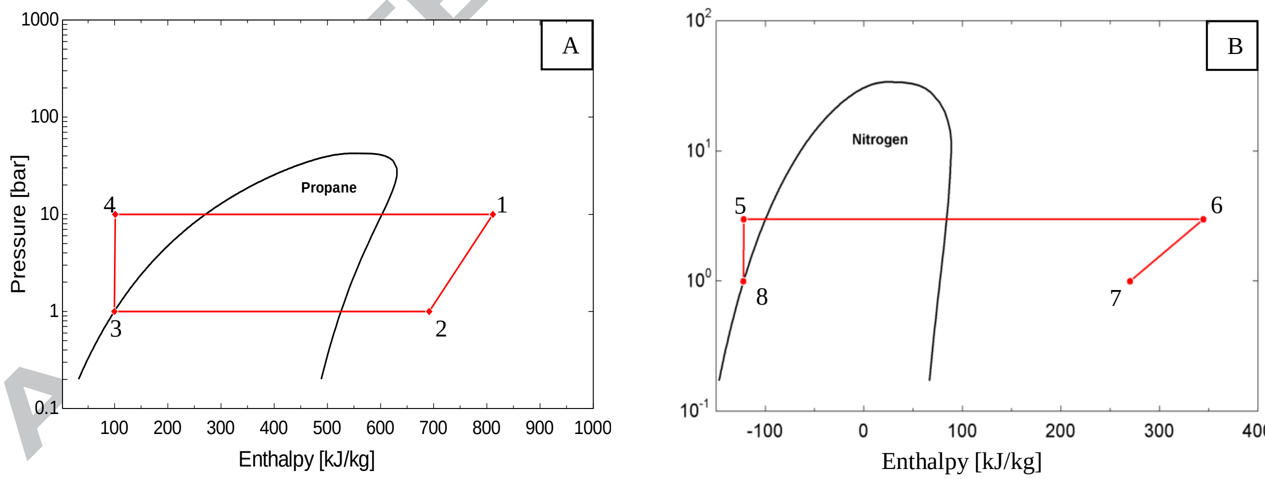

Fig.2. Thermodynamic pressure enthalpy diagram of hybrid open- Rankine cycle:- ; A topping part; B bottoming part

Table 2.
The hybrid open-Rankine cycle model input variable

Parameter	Unit	Value
Temperature of the heat source (T1)	K	400
Expander1 pressure ratio	—	10
Expander2 pressure ratio	—	1.5-3
Pumps efficiency	—	%80
Heat exchanger effectiveness	—	% 85

3. Expander development methodology

3.1 Preliminary design by the mean-line method

The main target for the preliminary design (PD) is to find the initial expander's passage dimensions and shapes such as the chord length (C), throat length (o), pitch width (S) and trailing and leading edge thickness details.[39]; The dimensionless coefficient's loading coefficient (Ψ) and reaction coefficient (R_n) have been used in the preliminary design to predict the expander's efficiency and produce the velocity triangle after calculating the velocity angles as clarified in Equations (9-12). [40]; the mean-line modelling technique has been used to develop the initial axial expander design, by assuming the change in the flow along a mean radius through the expander with span wise variations was neglected. Fig.3 shows the velocity triangle where the flow enters the stationary blades at absolute angle (α_1) and velocity (C1); then leaves the stationary blades at absolute angle (α_2) and velocity (C2). In the rotating blades the flow enters at relative angle (β_2) and velocity (w2); next the flow leaves the rotor blade at relative angle (β_3) and velocity (w3).

$$\tan\beta_2 = \frac{(\Psi - 2R_n)}{2\varphi} \tag{9}$$

$$\tan\beta_3 = -\frac{(\Psi + 2R_n)}{2\varphi} \tag{10}$$

$$\tan\alpha_2 = -\frac{(\frac{\Psi}{2} - (1 - R_n))}{\varphi} \tag{11}$$

$$\tan\alpha_1 = \frac{(\frac{\Psi}{2} + (1 - R_n))}{\varphi} \tag{12}$$

Soderberg's correlation has been used to estimate the losses for the expander's blade, where this correlation depends on the optimum ratio of pitch-to-chord or what is called Zweifel's ratio. The losses criteria deal with expander's dimensions ratios such as pitch space to chord; aspect ratio (axial cord/blade height); and Reynolds number, as in Equations (13-17) and stated in [41]:-

$$\epsilon = \alpha_1 + \alpha_2 \tag{13}$$

Where ϵ is the blade deflection angle and loss coefficient ζ_1 related to this deflection by the Horlock chart. [41];

$$\zeta_2 = (1 + \zeta_1)\left(0.975 + 0.075\frac{b}{H}\right) - 1 \tag{14}$$

And for the Reynolds numbers other than 10^5

$$\zeta_3 = \left(\frac{10^5}{Re}\right)^{1/4} \zeta_2 \tag{15}$$

Calculating static to total efficiency and total to total efficiency determined by:

$$\eta_{ts} = \left[1 + \frac{\zeta_R w_3^2 + \zeta_S C_2^2 + C_1^2}{2w}\right]^{-1} \tag{16}$$

$$\eta_{tt} = \left[1 + \frac{\zeta_R w_3^2 + \zeta_S C_2^2}{2w}\right]^{-1} \tag{17}$$

This model has been developed with the engineering equations solver software (EES) using inlet conditions (pressure, temperature, mass flow rate). The initial small-scale axial expander design geometry outputs from the PD EES code is shown in Table 3.

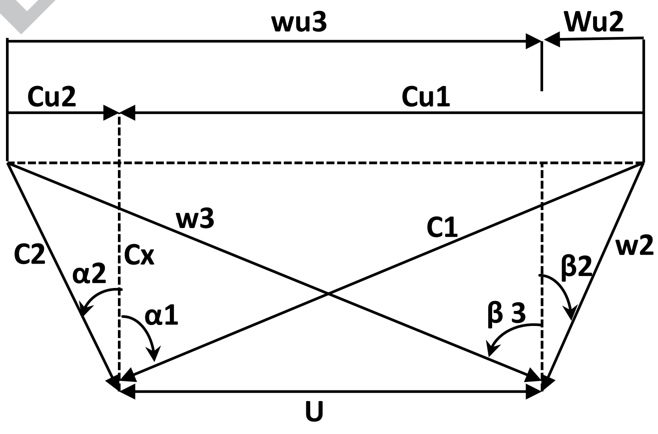

Fig.3. Velocity diagram for one stage axial expander

Table 3
Output parameters for preliminary design PD algorithm.

Parameter	units	Value
Tip radius	mm	36
Hub radius	mm	30
Blade height	mm	6
Rotor		
Inlet blade angle	degree	-25
Outlet blade angle	degree	60
Stagger angle	degree	35
Number of blade	——	35
Blade cord	mm	7
Tip clearance	mm	0.5
Stator		
Inlet blade angle	degree	-20
Outlet blade angle	degree	55
Stagger angle	degree	35
Number of blade	——	40
Blade cord	mm	8

3.2 CFD model

The initial design was developed by the mean-line method can be further improved through 3D CFD analysis. The CFD simulation was carried out using ANSYS CFX 17.0 which has the ability to solve 3D compressible flow. Fig. 4 shows the flow diagram used for the CFD analysis where the output from the PD has been used as input to the CFD analysis. In the ANSYS software, the blade generation has been carried out using the BladGen module, which requires the blade geometry to be defined in terms of its tip radius, hub radius, axial cord and the blade angles at the hub, mid-span and shroud sections. The resulting 3D CAD design is shown in Fig. 5. The second step is to import the geometry to the TurboGrid module for automatic meshing using structured hexahedral mesh with sweep or multi-zone suitable for any complex geometry. Also, the mesh adjacent to the blade wall was designed by using the proportional to mesh size method, where the factor ratio 3 is selected to get the y+ value near to unity. For the rotor, the tip clearance value was specified in the shroud tip details section. The mesh structure is shown in Fig. 6; where it is clear that a mesh size of 800,000 nodes gives stable solutions.

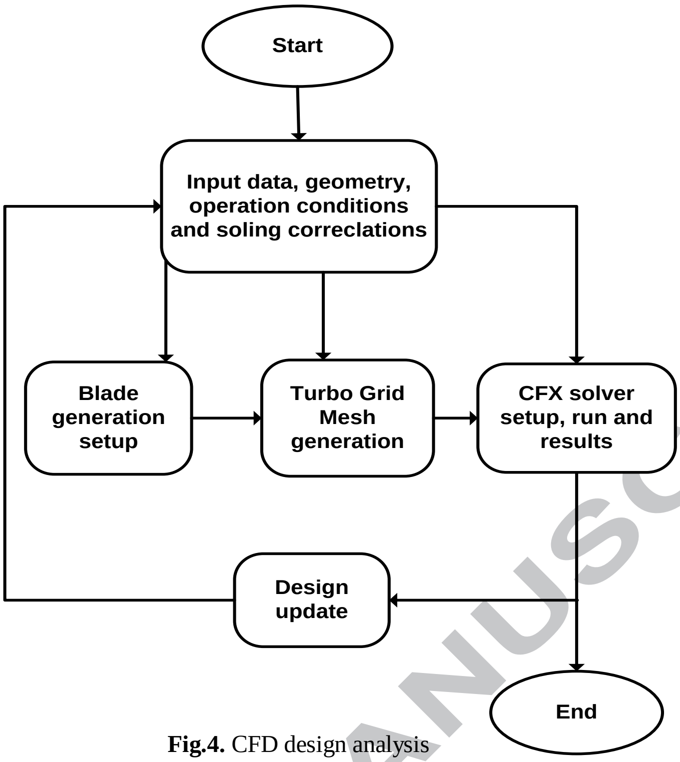

Fig.4. CFD design analysis flowchart

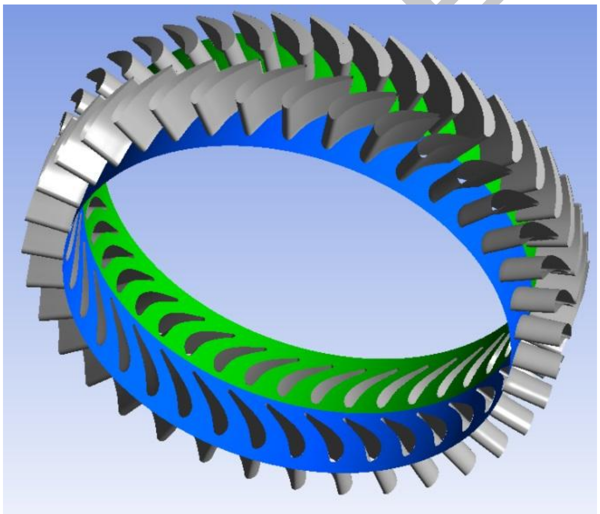

Fig. 5. One stage small scale axial turbine 3D geometry

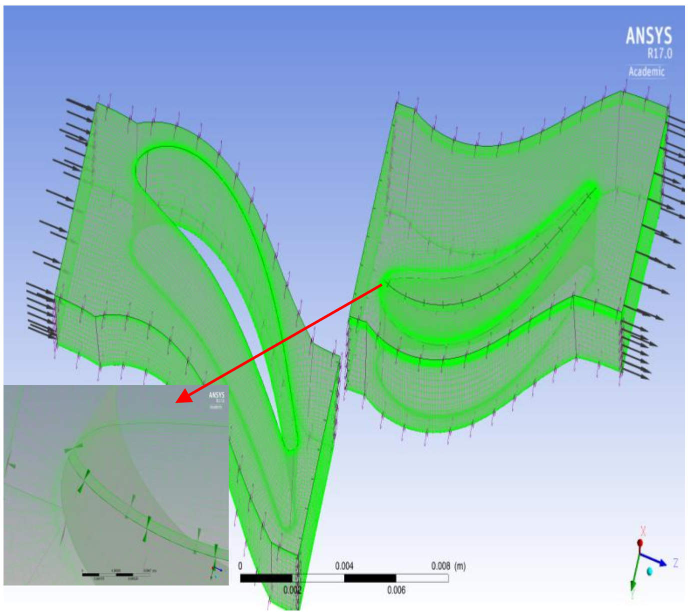

Fig.6. Mesh size and structure

The third step in Fig. 4; is to import the mesh geometry into the CFX solver package with the boundary conditions from the mean-line modeling also the no-slip boundary and periodic conditions are selected to determine flow direction. The working fluid is chosen from the list of materials in the CFX pre-post tree which is in this work is nitrogen. The staged mixing-plan model has been selected to model the interface between the stator outlet and rotor inlet domains. This model performs a circumferential averaging of the fluxes through bands on the interface instead of assuming a fixed relative position of the components. The shear stress transport (k-ω SST) turbulence model is used to evaluate the flow separation from the blade surface by capturing the turbulence enclosure of the first node near the wall. This model combines the k-ε and k-ω turbulent models to accurately model a wide range of applications. [42, -43]; The automatic near wall functions have been used because they transition gradually between the wall functions and the sublayer according to grid density. The k-ω turbulence model transport equations calculate the specific dissipation rate (ω) and kinetic energy (k):-

$$\frac{\partial}{\partial t}(\rho k) + \frac{\partial}{\partial x_i}(\rho k u_i) = \frac{\partial}{\partial x_j}\left(\Gamma_k \frac{\partial k}{\partial x_j}\right) + G_k - Y_k + S_k \tag{18}$$

$$\frac{\partial}{\partial t}(\rho \omega) + \frac{\partial}{\partial x_i}(\rho \omega u_i) = \frac{\partial}{\partial x_j}\left(\Gamma_\omega \frac{\partial \omega}{\partial x_j}\right) + G_\omega - Y_\omega + S_\omega \tag{19}$$

Where Y_k and Y_ω are the fluctuating dilation of compressible turbulence; G_k and G_ω are the turbulent kinetic energy and dissipation generation term; S_k and S_ω are k-ω turbulence model source terms.

3.2.1 Validation

Due to a lack of experimental data for nitrogen small scale expanders, the Cambridge expander was used to validate the CFD modeling procedure of this work. The Cambridge expander was developed using the design parameters shown in Table 4 by Denton [44] with air as the working fluid. Fig. 7 shows the comparison between the CFD work and the measured results from the Cambridge expander; where the difference between the experimental data and CFD prediction of the loss coefficient average value is 9.4%. The efficiency calculated from the experimental data was 93.8%; while in the CFD, it was 94.11%.

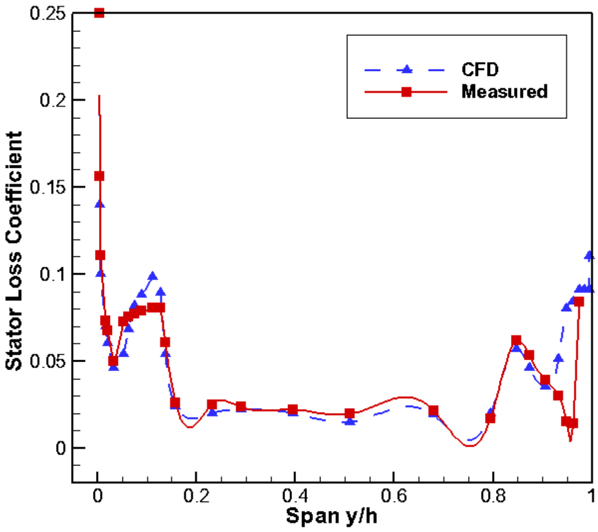

Fig. 7. Comparison for Cambridge low-speed expander stator between CFD work and measured data

Table 4.
Design parameters for Cambridge low-speed turbine

Parameter	Value
Flow rate	20.1 kg/s
Angular Velocity	525 RPM
Inlet total pressure	101.3 Kpa
Inlet total temperature	293 K
Hub diameter	533.4 mm
Tip diameter	762.0 mm
Tip clearance	0.63 mm
Axial chord	106.1 mm
Number of blades for stator	36
Number of blades for rotor	51

4. CFD 3D optimization

To develop an optimal cryogenic expander design a trade-off has to be accepted to compare different expander geometries to find the best design for specific goals and conditions. The process of preparing the optimization is known as problem formulation; which is intended to identify the design variables, objective functions, constraints, and optimization algorithm [45]. The change of any blade geometry parameter makes a considerable change in the losses in terms of total pressure through the turbine stage so that always there is an optimum value for each parameter that achieves minimum losses. To achieve the optimum profile for an expander blade, the highest expander efficiency and the required power, these parameters need to be optimized simultaneously.

Figure 8 shows the flow chart of the expander's optimization process including the use of design exploration optimization (DEO) module. In the first step, the mean-line analysis has been used to develop an initial design of the cryogenic expander, which will then be imported to BladeGen, Turbo Mesh and CFX modules in ANSYS; these were used to carry out the 3D CFD analysis in order to predict the performance of this initial design. To optimize the expander, the geometry generated by the BladGen module in the initial CFD analysis must be exported to the design module (DM). The DM then enables the selection of the design parameters required for optimizing the geometry. Two types of design parameters need to be considered, namely input and output design parameters. The input design parameters include blade geometry parameters such as trailing edge thickness and also boundary conditions, such as mass flow rate, with their minimum and maximum values. The output design parameters include power and efficiency that are produced after solving the model with input design parameters. To proceed with the optimization, the output from the DM CFD model has exported to the design of experiments (DoE) module.

The design of experiments (DoE) module will divide the range of the selected input parameters into a number of divisions or steps. Then it will use a combination of all the steps of the input parameters to generate a matrix of design configurations; which will then be simulated using the CFX. The output of the DoE process is then inputted to the response surface module (RSM) which develops relationships between the selected input and output parameters. In the response surface module (RSM) the second-order (quadratic) response surface is typically used as shown in Eq. 20 [46]:

$$Y = \beta_o + \sum_{i=1}^{k} \beta_i x_i + \sum_{i=1}^{k} \beta_{ii} x_i^2 + \sum_{i=1}^{k-1} \sum_{j=2}^{k} \beta_{ij} x_i x_j \ + \nu \qquad (20)$$

Where x is an independent variable; β is a regression coefficient and ν is the random error. These relationships are then used by the optimization module to determine the expander's design that produces the maximum output. In the optimization module, which is the final step in Fig. 8, the user defined objective functions, constraints and the type of the optimization method will all be used to produce the final optimum design.

In the expander's design optimization, it is recommended that all parameters of the geometry are adequately defined and restricted to the quantity required for better blade profile representation. This work describes camber line control point's parameterization technique, which generates a flexible curve with control points (x, y). In this geometry definition method, both pressure and suction sides of the turbine are defined with respect to the camber line, which is identified as shown Figs. 9. In these figures, the positions where the thickness and angle have been varied in the case of the stator blade and the rotor blade respectively are portrayed. For the stator, the selected positions are 5 for the angle (SA1 to SA5) and 7 for the thickness (ST1 to ST7) as shown in Fig.9A. For the rotor blade, 5 positions were selected for varying the angle (RA1 to RA5) and 6 positions for varying the blade thickness (RT1 to RT6) as shown in Fig.9B. In the process of selecting these positions, the control points at the hub section will update the other blade sections along the blade span automatically; this will decrease the number of design parameters along the blade span.

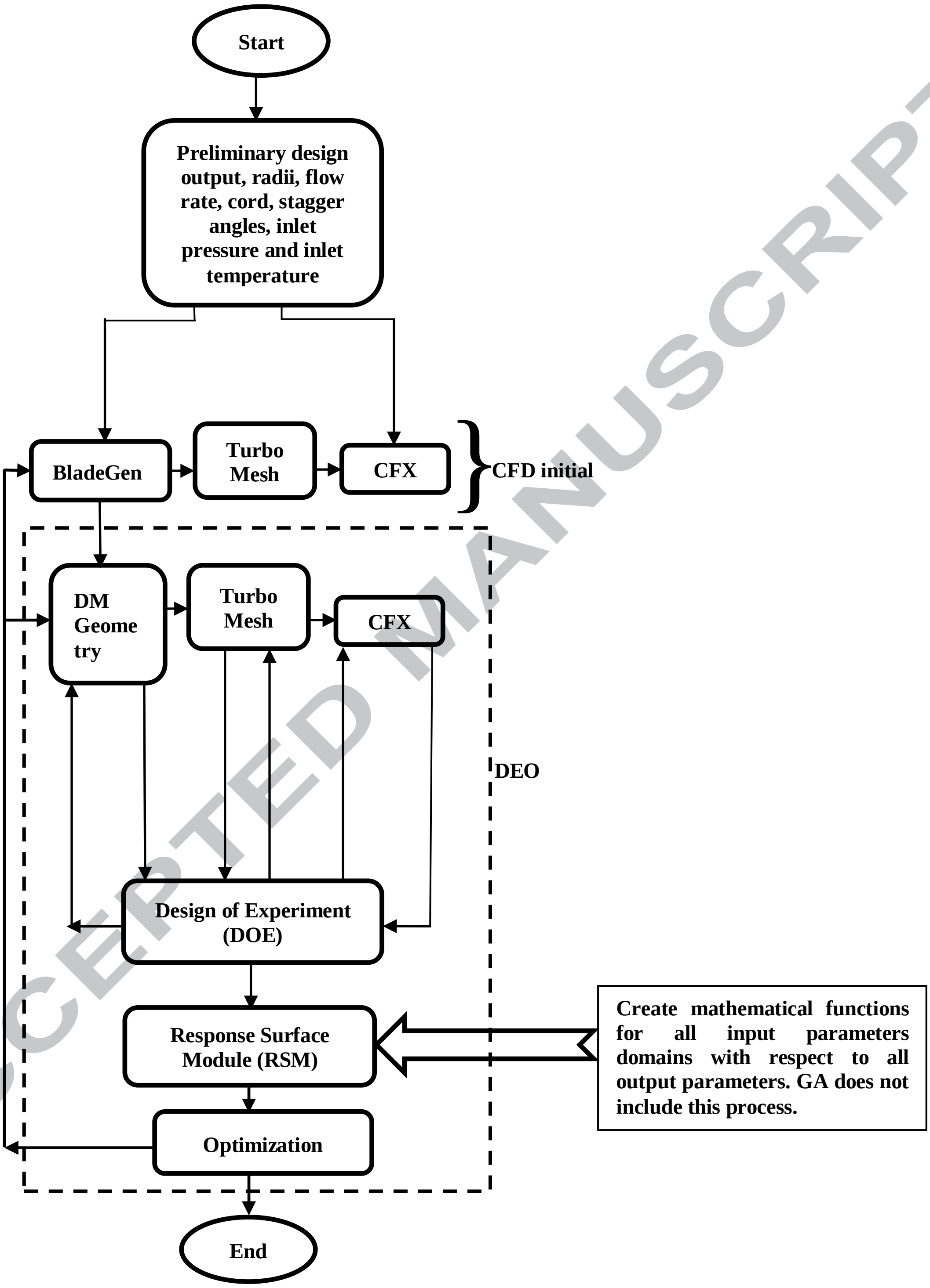

Fig.8. Design exploration optimization steps

In addition, the rotor and stator blades' trailing edge thickness, leading edge thickness, the number of blades and tip clearance have also been used as input design parameters. The DOE methods used in this work are the central composite design (CCD) and the custom methods because they are more flexible than other methods and cover a wide range of design configurations. The RS scheme selected in this work is the standard response surface full 2nd-order polynomial algorithm which gives an approximation of the true input-to-output relationship. The multi-objectives genetic algorithm (MOGA) has been selected as the optimization method since it allows the use of more than one objective for the optimization process [46]. In the Genetic Algorithm GA method, the software solves for every single point (step) in the input parameters domain (like a number of blades, trailing edge thickness and tip clearance) and generates a matrix of output solutions relating all out parameters (like power output and efficiency) to their relevant input parameters values. Then it searches for the optimum combinations of input and output values, a process that takes very long computational time and does not include the intermediate values between the specified steps of the input parameters values. The MOGA method uses the response surface module (RSM) which creates mathematical functions for all input parameters domains with respect to all output parameters, then carries the optimization process for these functions. This approach allows for including all input parameters domain points in the optimization process, thus giving a more accurate solution. Also, it requires less computational time, since it does not perform the optimization process for every single point of the input parameters domain as in the GA process.

The above represents a fully detailed explanation for 3D optimization of a small-scale axial expander by the camber line control point's parametrization technique; which is explained in this way for the first time to enrich the lack of knowledge in this turbomachinery area; which is describe the blade thickness and angle are varied at various positions along the camber line of the blade.

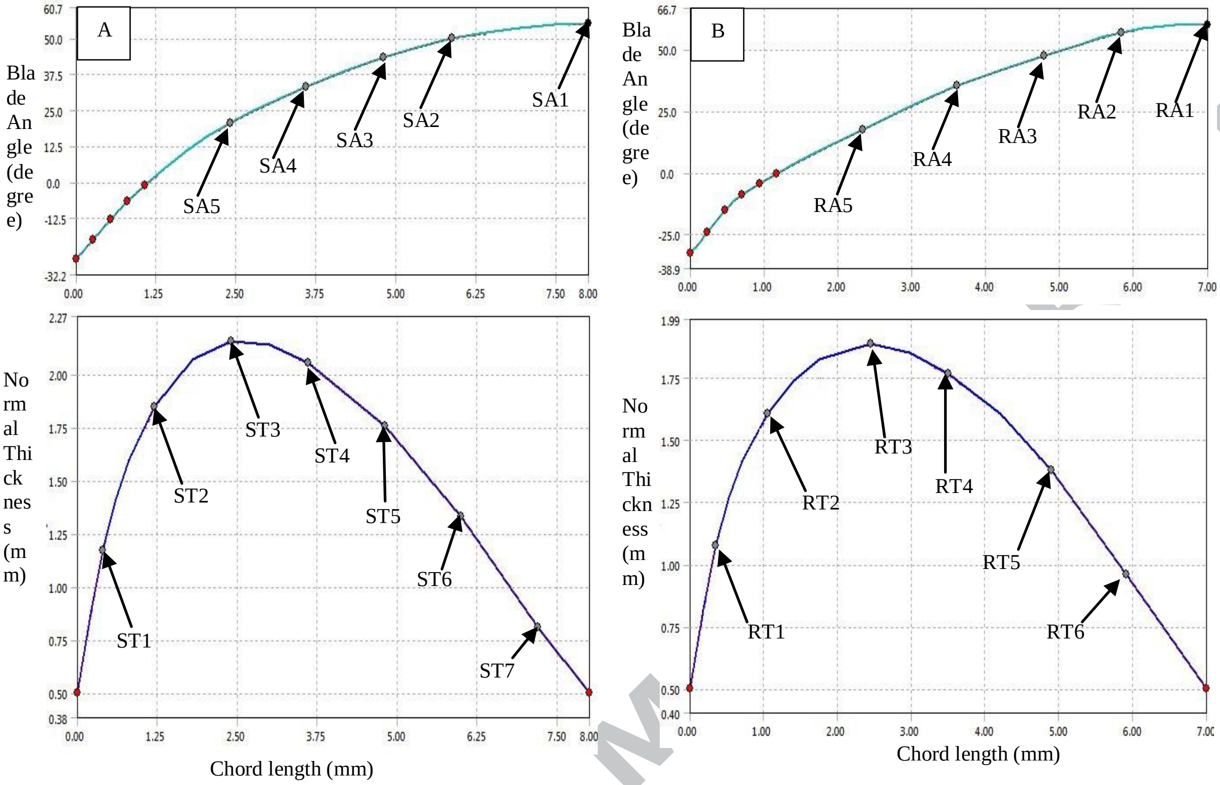

Fig.9. Angle and thickness design variable distributed on the camber line, A Stator , B Rotor

4. Results and discussion

The CFD simulation has been carried out to optimize the performance of a small-scale cryogenic axial expander with a hybrid open-Rankine cycle. Fig.10 show the effect of varying angles along the positions (SA1 to SA5 and RA1 to RA5) of the stator and rotor camber line profiles on the expander's efficiency and power output. This figure shows that there is an optimum angle for each position. For example, position RA5 for the rotor has a higher efficiency than the others because it is in the middle of the rotor blade leading to a more significant effect on the rotor blade's shape.

Fig. 11 show the effect of varying the blade thickness along the camber line positions of the rotor (RT1, RT3, RT5, RT6) and stator (ST1, ST3, ST5, ST7) on the expander's efficiency and power output. These figures show that increasing the blade thickness will decrease the expander's efficiency and power output. Also, it is clear that position ST1 on the stator and RT6 on the rotor have a lower impact on the efficiency. Fig. 12 shows the effect of varying the stator and the rotor trailing edge thicknesses on the expander's efficiency and power output. These figures show that increasing the trailing edge thickness of the stator and rotor will decrease the efficiency and power as reported by [47].

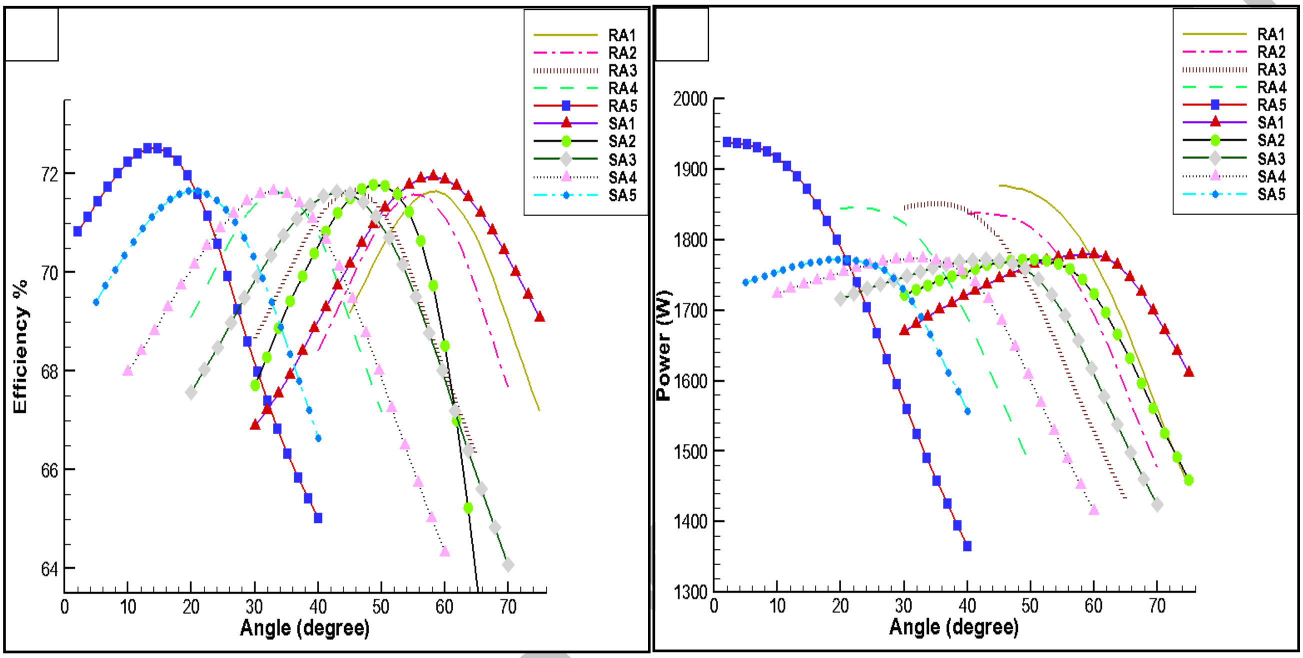

Fig. 10. Effect of control points angle parameters on A efficiency , B power

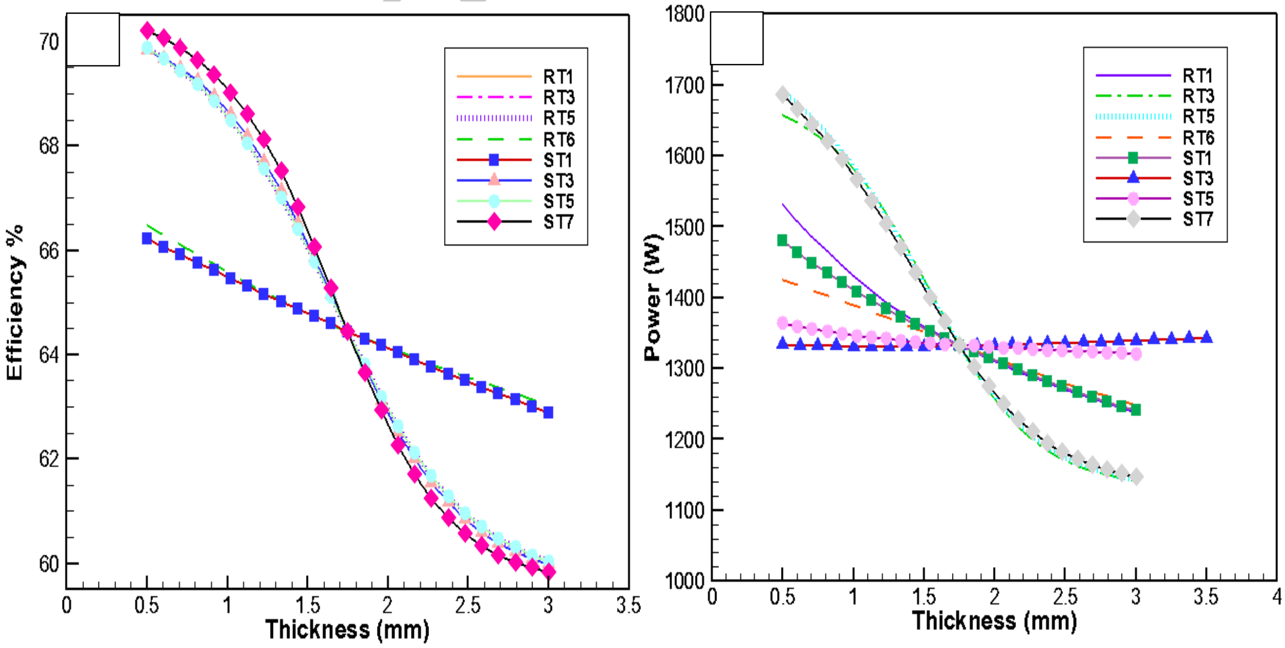

Fig. 11. Effect of control points thickness parameters on A efficiency , B power

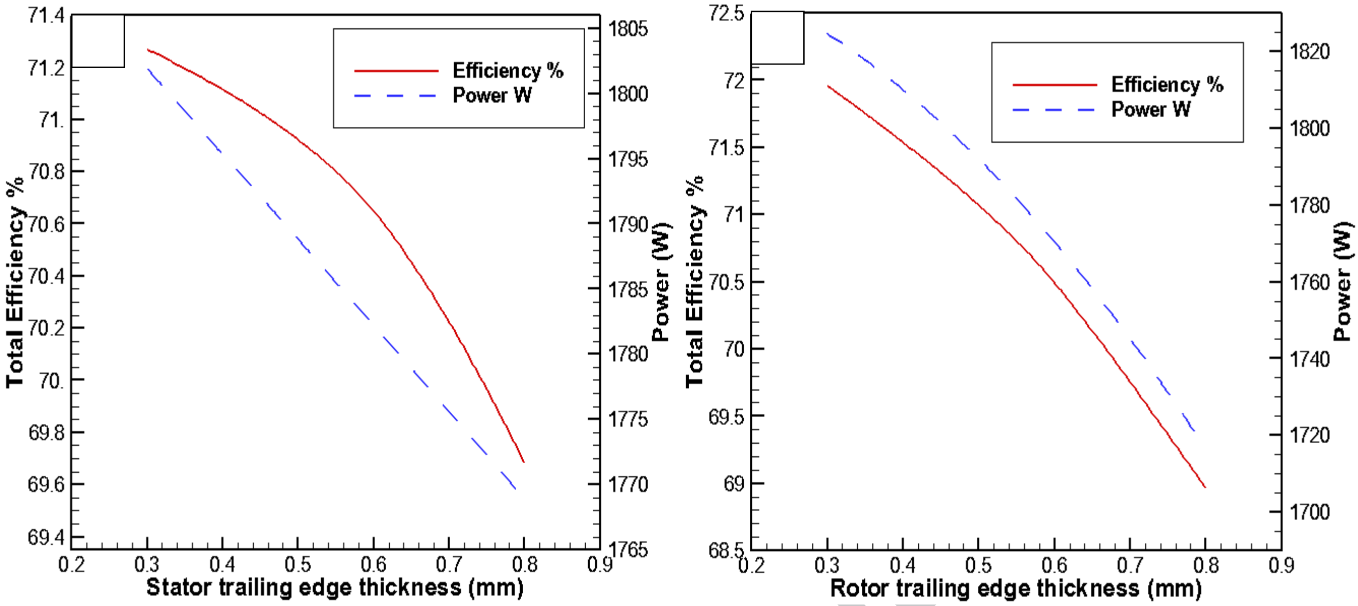

Fig. 12. Effect of the trailing edge thickness on power and efficiency A stator, B Rotor

The parameterization was conducted by the camber line control points' technique for the rotor and stator. Table 5 compares the staged geometrical parameters of the optimized design to the initial design produced by the CFD work; while Fig. 13 compare the blades' profile for the two cases. It can be seen that the optimized stator and rotor profiles have shorter chord lengths, thinner leading edges and smaller curvature leading to lower losses and higher efficiency.

Table 5.
Design variables' optimization results

Variable Parameter	Old Value	Optimum Value
Stator number of blade	40	36
Rotor number of blade	35	39
Stator trailing edge thickness (mm)	0.5	0.3
Stator leading edge thickness (mm)	0.5	0.45
Rotor trailing edge thickness (mm)	0.5	0.3
Rotor leading edge thickness (mm)	0.5	0.31
Shroud tip clearance (mm)	0.5	0.3

Fig. 14 shows the comparison for pressure distribution along the rotor passage for optimum and baseline blade design at span 50%; the lowest pressure location corresponds to the location of the passage throat where the velocity is highest. The work done by the expander is provided by the blade loading where the area enclosed by pressure and the suction side curves represents the net torque. It is obvious from Fig.14 that the loading in the optimum blade case is better than the baseline blade design, where the flow accelerated more on the suction side.

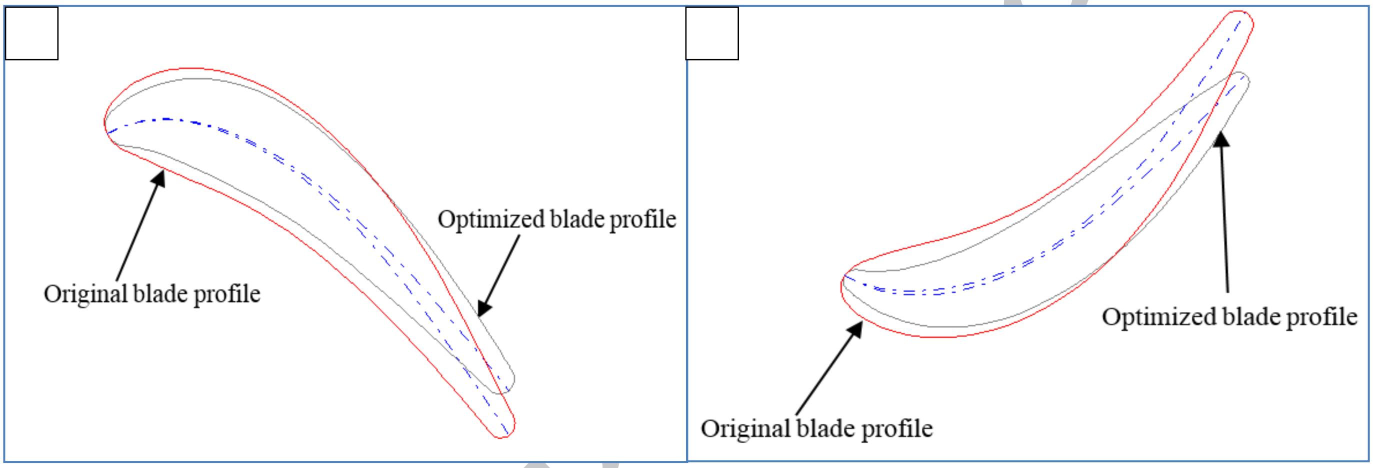

Fig. 13. Comparison between old and new rotor blade profile A Stator, B Rotor

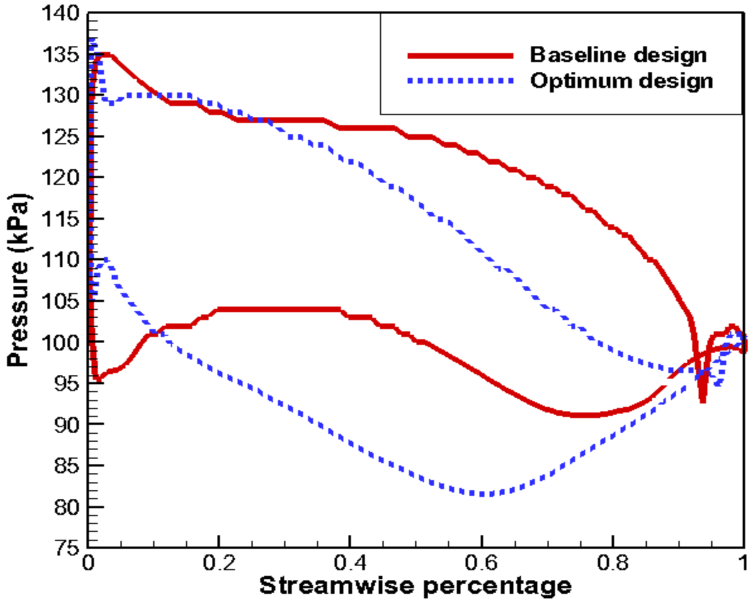

Fig. 14. Rotor blade loading at 50% span for baseline and optimum blade design

The losses in the expander are always affected by the blade shape, such as the angle and thickness distribution and moreover the leading, trailing and tip clearance thickness. However, the generation of these losses can be described by entropy formation, as shown in Fig.15; This figure shows the entropy contour for optimum and baseline full stage designs at 50% span comparison between the optimum and baseline underlines the decreasing entropy generation with optimum geometry, which minimizes the aerodynamic blade losses. Fig. 16 compares the expander's efficiency for the original and optimized design at rotational speeds ranging from 10000 RPM to 70000 RPM. It can be seen that the overall expander's efficiency of the optimized design is higher than that of the original design at all rpms, with a maximum improvement of 8% at 70000 RPM. Such results emphasize that the optimum design geometry gives a good performance not only at the design point but also with off-design points.

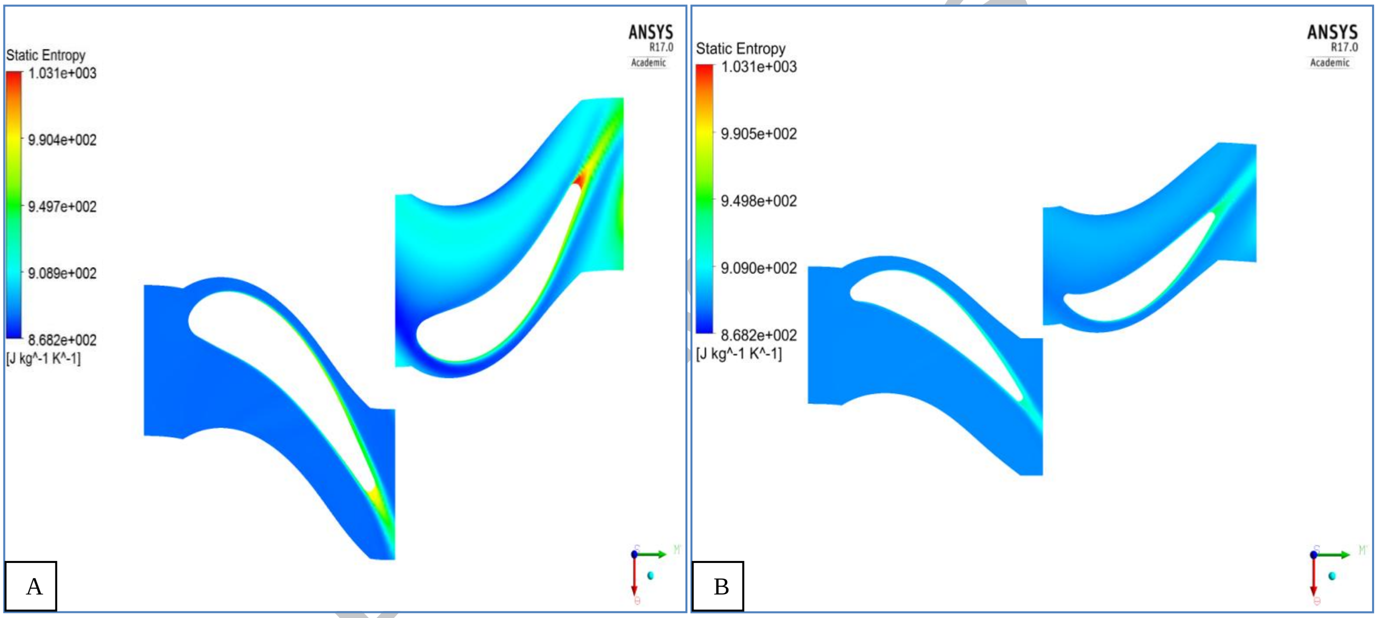

Fig. 15. Entropy contour at 50% span for A baseline and B optimum blade design

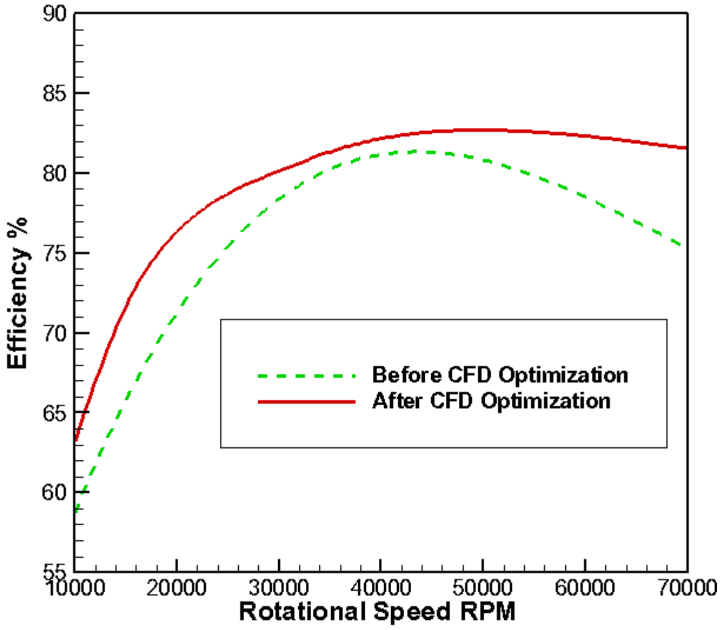

Fig. 16. Comparison between original design and optimum design for rotor multi rotational speed

6. Results of open-Rankine cycle analysis

Using the hybrid open-Rankine cycle analysis in Eqs (1)-(8) to estimate the cycle's efficiency for various operating conditions is shown in Fig. 17. The cycle's thermal efficiency with the optimum nitrogen expander's design reaches 26.57%. This enhancement in the cycle's efficiency is based on the expander's isentropic efficiency, delivered from 3D CFD optimization and put into hybrid open-Rankine cycle modeling. Fig 18 shows the effect of expander efficiency on the thermodynamic properties during the expansion process where process 6 to 7 is at expander efficiency 40% and process 6 to 7^* is at expander efficiency of 76.3%. Fig.18A shows that at same outlet pressure of 1 bar the enthalpy for point 7 is more than that of point 7^* which means that in the case of point 7 more energy is rejected without producing work output which in turn decreases the efficiency of the cycle. Also Fig18B shows that point 7 has higher temperature than point 7^* and the entropy at point 7 is greater than point 7^* thus increasing the losses in the expander and the cycle. These results are better than in previous studies [35-36] in terms of the low flow rate of 0.1kg/s and low rotational speed of 2000 rpm. This study discloses the potential of introducing an optimization technique to solve difficult operational conditions like low flow rate and rotational speed in small-scale expander's design.

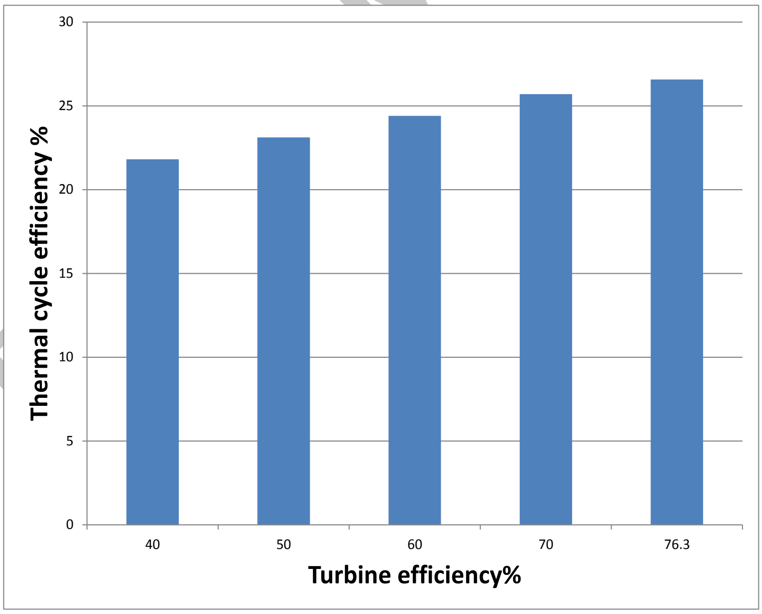

Fig. 17. Effect of the cryogenic turbine efficiency on hybrid cycle thermal efficiency

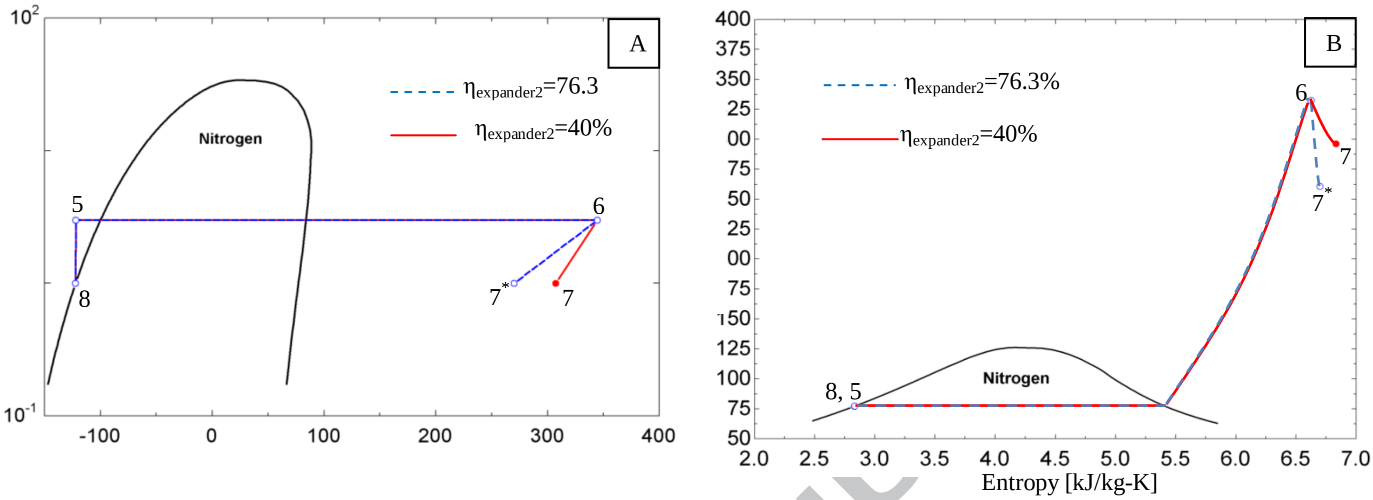

Fig.18. Comparison for thermodynamic properties of hybrid open- Rankine cycle at different expander efficiencies: - ; A pressure enthalpy; B Temperature entropy

7. Conclusions

Three-dimensional optimization for a nitrogen small-scale turbine has been developed using a novel camber line control point parameterization technique. The newly developed expander was used to improve the overall efficiency of the proposed hybrid open-Rankine cycle. The turbine's design phase starts with thermodynamic cycle analysis using the EES program in order to identify the expander's specifications. Based on the thermodynamic cycle analysis, a small turbine was designed using a mathematical 1D mean-line approach followed by 3D CFD modeling. For a more efficient turbine design, 3D CFD modeling coupled with MOGA optimization was conducted. The main conclusions of this work can be summarized as follows:

- The 3D CFD turbine optimization using the camber line control point parameterization technique has been proven as a powerful design approach to achieve a highly efficient turbine and could improve mean-line turbine efficiency from 72% to 76.34%
- The optimized developed turbine could improve the overall thermal cycle efficiency significantly by 3.38% compared to baseline turbine design results, leading to better cycle performance levels.
- The combination of the open expansion cycle and the Rankine cycle can enhance the thermal cycle efficiency of the hybrid open-Rankine cycle by 11.42%.

Acknowledgment

The main author (Khalil M. Khalil) gratefully acknowledges the Higher Committee for Education Development in Iraq HCED for funding my Ph.D. scholarship at the University of Birmingham, the UK which facilitates the continuation of research on 3D optimization of nitrogen small-scale expanders.

Nomenclature

Greek symbols

α	absolute flow angle (degree)
β	relative flow angle (degree)
ζ	loss coefficient (-)
η	efficiency (-)
ρ	fluid density (kg/m3)
ϵ	Blade deflection angle (degree)
φ	flow coefficient (-)
$\boldsymbol{\Psi}$	loading coefficient (–)

Symbols

b	axial cord length (mm)
C	absolute velocity (m/sec)
E	heat exchanger effectivness(-)
h	enthalpy (J/kg)
H	blade height (mm)
k	turbulent kinetic energy (m^2/ s^2)
Q	heat rate (J/s)
q	specific heat (J/kg)
R_n	reaction (-)
Re	Reynolds number (-)
t	Time (s)
T	Temperature (K)
W	specific work (kJ/kg)
w	relative velocity (m/s)

Subscript

1-8	stations within the cycle respectively
ts	Total to static
tt	Total to total
S	stator
R	rotor

Acronyms

CAES	compressed air energy storage
CES	cryogenic energy storage
CFD	computational fluid dynamics
LASE	liquid air storage energy
PD	preliminary design
PSH	pumped storage hydropower
SST	shear stress transport

References

[1] Ghoniem AF. Needs, resources and climate change: clean and efficient conversion technologies. Progress in Energy and Combustion Science. 2011 Feb 28;37(1):15-51

[2] Dodds PE, Garvey SD. The Role of Energy Storage in Low-Carbon Energy Systems. Storing Energy: with Special Reference to Renewable Energy Sources. 2016 Apr 11:1.

[3] Huff G, Tong N, Fioravanti R, Gordon P, Markel L, Agrawal P, Nourai A. Characterization and assessment of novel bulk storage technologies: a study for the DOE Energy Storage Systems program. Sandia National Laboratories; 2011 Apr 1.

[4] Luisa F. Cabeza, Ramteem S., Jinyue Y. Handbook of Clean Energy Systems. Wiley . 2015.

[5] Ameel B, T'Joen C, De Kerpel K, De Jaeger P, Huisseune H, Van Belleghem M, De Paepe M. Thermodynamic analysis of energy storage with a liquid air Rankine cycle. Applied Thermal Engineering. 2013 Apr 5;52(1):130-40.

[6] Rahbar K, Mahmoud S, Al-Dadah RK, Moazami N. Parametric analysis and optimization of a small-scale radial turbine for Organic Rankine Cycle. Energy. 2015 Apr 1;83:696-711.

[7] Al Jubori A, Daabo A, Al-Dadah RK, Mahmoud S, Ennil AB. Development of micro-scale axial and radial turbines for low-temperature heat source driven organic Rankine cycle. Energy Conversion and Management. 2016 Dec15;130:141-55.

[8] Qiang W, Yanzhong L, Jiang W. Analysis of power cycle based on cold energy of liquefied natural gas and low-grade heat source. Applied thermal engineering. 2004 Mar 31;24(4):539-48.

[9] Feifei B, Zhang Z. Integration of low-level waste heat recovery and liquefied nature gas cold energy utilization. Chinese Journal of Chemical Engineering. 2008 Feb 29;16(1):95-9.

[10] Li Y, Chen H, Ding Y. Fundamentals and applications of cryogen as a thermal energy carrier: a critical assessment. International Journal of Thermal Sciences. 2010 Jun 30;49(6):941-9.

[11] Guizzi GL, Manno M, Tolomei LM, Vitali RM. Thermodynamic analysis of a liquid air energy storage system. Energy. 2015 Dec 15;93:1639-47.

[12] Li Y, Wang X, Jin Y, Ding Y. An integrated solar-cryogen hybrid power system. Renewable energy. 2012 Jan 31;37(1):76-81.

[13] Chen H, Ding Y, Peters T, Berger F, inventors; Highview Enterprises Limited, assignee. Energy storage and generation. United States patent application US 12/280,739. 2007 Feb 27.

[14] Khalil KM, Ahmad A, Mahmoud S, Al-Dadah RK. Liquid air/nitrogen energy storage and power generation system for micro-grid applications. Journal of Cleaner Production. 2017 Jun 30.

[15] Kishimoto K, Hasegawa K, Asano T. Development of generator of liquid air storage energy system. Mitsubishi Juko Giho. 1998;35:60-3.

[16] Li Y, Wang X, Ding Y. A cryogen-based peak-shaving technology: systematic approach and techno-economic analysis. International Journal of Energy Research. 2013 May 1;37(6):547-57.

[17] Kantharaj B, Garvey S, Pimm A. Compressed air energy storage with liquid air capacity extension. Applied Energy. 2015 Nov 1;157:152-64.

[18] Li Y, Cao H, Wang S, Jin Y, Li D, Wang X, Ding Y. Load shifting of nuclear power plants using cryogenic energy storage technology. Applied Energy. 2014 Jan 31;113:1710-6.

[19] Abdo RF, Pedro HT, Koury RN, Machado L, Coimbra CF, Porto MP. Performance evaluation of various Cryogenic energy storage systems. Energy. 2015 Oct 31;90:1024-32.

[20] Li Y, Jin Y, Chen H, Tan C, Ding Y. An integrated system for thermal power generation, electrical energy storage and CO2 capture. International Journal of Energy Research. 2011 Oct 25;35(13):1158-67.

[21] Morgan R, Nelmes S, Gibson E, Brett G. Liquid air energy storage– Analysis and first results from a pilot scale demonstration plant. Applied Energy. 2015 Jan 1;137:845-53.

[22] Smith EM. Storage of electrical energy using supercritical liquid air.Proceedings of the Institution of Mechanical Engineers. 1977 Jun 1;191(1):289-98.

[23] Darcovich K, Entchev E. An International Survey of Electrical and DHW Load Profiles for Use in Simulating the Performance of Residential Micro-cogeneration Systems. ECB Annex. 2014;54.

[24] Khalil KM, Mahmoud S, Al-Dadah RK. Impact of advanced blade configuration on small scale cryogenic axial turbine performance. InStudents on Applied Engineering (ICSAE), International Conference for 2016 Oct 20 (pp. 248-253). IEEE. [25] Song P, Wei M, Shi L, Danish SN, Ma C. A review of scroll expanders for organic Rankine cycle systems. Applied Thermal Engineering. 2015 Jan 22;75:54-64.

[26] Khalil K, Mahmoud S, Al-Dadah RK, Fadhel AM. Parametric analysis of blade configurations for a small-scale nitrogen axial expander with hybrid open-Rankine cycle. Energy Conversion and Management. 2017 Jun 15;142:82-94.

[27] Morini M, Pavan C, Pinelli M, Romito E, Suman A. Analysis of a scroll machine for micro ORC applications by means of a RE/CFD methodology. Applied Thermal Engineering. 2015 Apr 5;80:132-40.

[28] Chang JC, Chang CW, Hung TC, Lin JR, Huang KC. Experimental study and CFD approach for scroll type expander used in low-temperature organic Rankine cycle. Applied Thermal Engineering. 2014 Dec 22;73(2):1444-52.

[29] Lemort V, Quoilin S, Cuevas C, Lebrun J. Testing and modeling a scroll expander integrated into an Organic Rankine Cycle. Applied Thermal Engineering. 2009 Oct 31;29(14):3094-102.

[30] Wang H, Peterson RB, Herron T. Experimental performance of a compliant scroll expander for an organic Rankine cycle.

[31] Qiu G, Liu H, Riffat S. Expanders for micro-CHP systems with organic Rankine cycle. Applied Thermal Engineering. 2011 Nov 30;31(16):3301-7.

[32] Craig HR, Cox HJ. Performance estimation of axial flow turbines. Proceedings of the Institution of Mechanical Engineers. 1970 Jun 1;185(1):407-24.

[33] Qin X., Chen L., Sun F. and Wu C., 2003. Optimization for a steam turbine stage efficiency using a genetic algorithm. Applied thermal engineering, 23(18), pp.2307-2316.

[34] Ennil AB, Al-Dadah R, Mahmoud S, Rahbar K, AlJubori A. Minimization of loss in small scale axial air turbine using CFD modeling and evolutionary algorithm optimization. Applied Thermal Engineering. 2016 Jun 5;102:841-8.

[35] Rahbar K, Mahmoud S, Al-Dadah RK, Moazami N. One-dimensional and three-dimensional numerical optimization and comparison of single-stage supersonic and dual-stage transonic radial inflow turbines for the ORC. InASME 2016 Power Conference collocated with the ASME 2016 10th International Conference on Energy Sustainability and the ASME 2016 14th International Conference on Fuel Cell Science, Engineering and Technology 2016 Jun 26 (pp. V001T08A017-V001T08A017). American Society of Mechanical Engineers.

[36] Al Jubori A, Al-Dadah RK, Mahmoud S, Ennil AB, Rahbar K. Three dimensional optimization of small-scale axial turbine for low temperature heat source driven organic Rankine cycle. Energy Conversion and Management. 2016 Nov 3.

[37] Klein, SA Engineering equation solver. F-chart Software, Middleton,WI; 2013.

[38] Cengel YA, Boles MA. Thermodynamics: an engineering approach. Sea. 1994;1000:8862.

[39] Japikse D, Baines N. Introduction to turbomachinery. 1994.

[40] Dixon S.L. and Hall C. Fluid mechanics and thermodynamics of turbomachinery. Butterworth-Heinemann. 2013.

[41] Horlock JH. Axial flow turbines: fluid mechanics and thermodynamics. Krieger Pub Co; 1973 Jun 1.

[42] Carregal-Ferreira J, Holzwarth A, Menter FE, Luu A. Advanced CFD analysis of aerodynamics using CFX. AEA Technology GmbH, Otterfing. 2002:1-4.

[43] Thomas E, Florian M, wolfgang v. Ted-aj03-542 heat transfer predictions based on two-equation turbulence models. In proceedings of the. ASME/JSME thermal engineering joint conference 2003 (vol. 2003, no. 6, p. 366).

[44] Denton JD, Hirsch C. Throughflow calculations in axial turbomachines. AGARD Advisory Report; 1981.

[45] ANSYS 17 CFX-Solver Theory Guide.

[46] Kim JH, Choi JH, Husain A, Kim KY. Performance enhancement of axial fan blade through multi-objective optimization techniques. Journal of Mechanical Science and Technology. 2010 Oct 1;24(10):2059-66.

[47] Khalil KM, Mahmoud S, Al-Dadah RK, Al Jubori A, Rahbar K. Impact of Skin Friction, Tip Clearance and Trailing Edge Losses on Small Scale Cryogenic Axial Turbine Performance. In ASME Turbo Expo 2016: Turbomachinery Technical Conference and Exposition 2016 Jun 13 (pp. V008T23A033-V008T23A033). American Society of Mechanical Engineers.